Accepted Manuscript

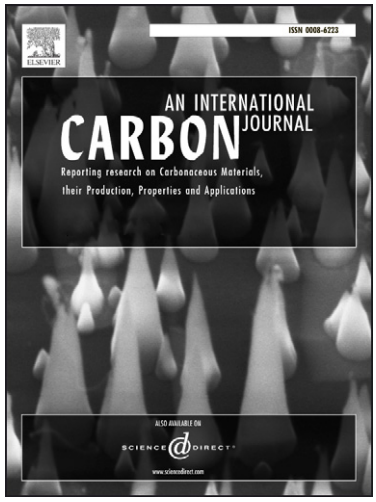

Direct synthesis of graphitic carbon nanostructures from saccharides and their use as electrocatalytic supports

M. Sevilla, C. Sanchís, T. Valdés-Solís, E. Morallón, A.B. Fuertes

PII: S0008-6223(08)00111-5
DOI: 10.1016/j.carbon.2008.02.019
Reference: CARBON 4809

To appear in: *Carbon*

Received Date: 19 September 2007
Revised Date: 21 February 2008
Accepted Date: 25 February 2008

Please cite this article as: Sevilla, M., Sanchís, C., Valdés-Solís, T., Morallón, E., Fuertes, A.B., Direct synthesis of graphitic carbon nanostructures from saccharides and their use as electrocatalytic supports, *Carbon* (2008), doi: 10.1016/j.carbon.2008.02.019

This is a PDF file of an unedited manuscript that has been accepted for publication. As a service to our customers we are providing this early version of the manuscript. The manuscript will undergo copyediting, typesetting, and review of the resulting proof before it is published in its final form. Please note that during the production process errors may be discovered which could affect the content, and all legal disclaimers that apply to the journal pertain.

ACCEPTED MANUSCRIPT

Direct synthesis of graphitic carbon nanostructures from saccharides and their use as electrocatalytic supports

M. Sevilla,[a] *C. Sanchís,*[b] *T. Valdés-Solís,*[a] *E. Morallón*[b] *and A. B. Fuertes*[*a]

[a] Instituto Nacional del Carbón (CSIC), P. O. Box 73, 33080-Oviedo, Spain

[b] Departamento de Química Física e Instituto Universitario de Materiales. Universidad de Alicante. Apartado 99. 03080-Alicante. Spain

[*] **Corresponding author.** E-mail**:** abefu@incar.csic.es

Abstract

An easy method is described for fabricating graphitic carbon nanostructures (GCNs) from a variety of saccharides; i. e. a monosaccharide (glucose), a disaccharide (sucrose) and a polysaccharide (starch). The synthesis scheme consists of: a) impregnation of saccharide with Ni or Fe nitrates, b) heat treatment under inert atmosphere (N_2) up to 900ºC or 1000ºC and c) oxidation in liquid phase to selectively recover the graphitic carbon. This procedure leads to GCNs with a variety of morphologies: nanopipes nanocoils and nanocapsules. Such GCNs have a high crystallinity, as shown by TEM/SAED, XRD and Raman analysis. The GCNs were used as supports for platinum nanoparticles, which were well dispersed (Mean Pt size ~ 2-3 nm). Electrocatalysts thus prepared have electrocatalytic surface areas in the 70-95 $m^2 \cdot g^{-1}$ Pt range and exhibit high catalytic activities towards methanol electrooxidation.

ACCEPTED MANUSCRIPT

1. Introduction

Carbon nanostructures with a graphitic framework, including the popular carbon nanotubes, have attracted widespread attention due to their applicability in numerous areas such as quantum electronic devices, electrocatalyst supports, electronic field emitters and electrode materials [1]. Arc discharge [2], laser vaporization [3] and plasma and thermal chemical vapour deposition [4] are typical methods employed to produce these materials. These procedures are complex and normally require very high temperatures (> 5000ºC), which makes them costly and limited in terms of scalability. For this reason, there is a growing interest in developing low-cost and facile synthetic processes. A simple method for preparing graphitic carbon nanostructures is the carbonization at moderate temperatures (<1000ºC) of carbon precursors in the presence of certain transition metals (Fe, Co, Ni, Mn, etc) that act as graphitization catalysts [5]. Catalytic graphitization has usually been performed through the carbonization of polymeric materials such as vinyl polymers, polyfurfuryl alcohol, resorcinol-formaldehyde gels and phenolic resins, which have been previously impregnated with a metallic salt [6-9].

We are undertaking a systematic investigation of different synthetic routes to produce, through catalytic graphitization, graphitic carbon nanostructures from a variety of precursors. Recently we reported the preparation of GCNs by using a cost-effective and widely available lignocellulosic material (sawdust) as precursor [10]. Likewise, we analyzed the use of commercially available iron or cobalt organic salts (i. e. Fe (II) gluconate and Co (II) gluconate) as precursors. These have the advantage of providing both the metal catalyst for the graphitization and the carbon source [11]. However, it is important to point out that the use of sawdust or gluconates as carbon precursor to fabricate GCNs has some limitations. Thus, sawdust is a complex lignocellulosic

ACCEPTED MANUSCRIPT

material that leads to a heterogeneous mixture of carbon nanostructures. On other hand, iron and cobalt gluconates are expensive compounds, which limits their applicability to large scale production of GCNs. In consequence, we are interested in identifying GCN precursors that allow overcoming these limitations. In this sense, saccharides are, in principle, good candidates. Indeed, they are pure materials that ensures homogeneous and reproducible GCNs and, in addition, they are inexpensive and widely available substances. Moreover, they have other interesting properties such as: a) they leave an important carbonaceous residue after pyrolysis, b) they have a high concentration of oxygen functional groups that suggest an easy and homogeneous impregnation and consequently a high dispersion of the metallic salts is expected. Based on these hypotheses, this work explores the use of three representative saccharides (glucose, sucrose and starch) as precursors for the synthesis of carbon nanostructures with a high crystallinity. The synthesis method employed to fabricate these nanostructures is similar to that described in our previous paper [10]. It consists in the thermal treatment, at a moderate temperatures (900-1000ºC), of the saccharides impregnated with metallic salts of Fe and Ni. In addition, we have investigated the application of such prepared graphitic nanostructures as supports for Pt nanoparticles and their electrocatalytic performance in fuel cell processes such as methanol oxidation.

2. Experimental

2.1 Synthesis of graphitic carbons

α-D-Glucose (96%, Aldrich), D(+)-sucrose (Rectapur, Prolabo) and potato starch (Sigma-Aldrich) were used as carbon precursors. These saccharides were impregnated with a solution of nickel or iron nitrate in ethanol (0.4 or 0.8 mmol metal·g^{-1} saccharide) and then heat-treated under nitrogen up to 900ºC or 1000ºC for 3 h (3ºC·min^{-1}). The samples thus obtained consisted of a mixture of metal nanoparticles, amorphous carbon

ACCEPTED MANUSCRIPT

and graphitic carbon nanostructures. In order to extract pure GCNs, the pyrolysed samples were dispersed in a solution of potassium permanganate with a composition (molar) of $H_2O/H_2SO_4/KMnO_4$ = 1:0.02:0.006 and refluxed for 2 h. The solid products were separated by centrifugation and washed with abundant distilled water. Finally, the precipitate was treated with 10 % HCl to remove the MnO_2. The recovered graphitic carbon samples were denoted as CX-nM-T, where X = A, G or S depending on the saccharide (A = starch, G = glucose and S = sucrose), n = metal amount (1 = 0.4 mmol metal·g^{-1} saccharide and 2 = 0.8 mmol metal·g^{-1} saccharide), M = the metal catalyst (Ni or Fe) and T = the temperature used during the heat treatment (900ºC or 1000ºC).

2.2. Preparation of Pt/GCN electrocatalysts and electrochemical measurements

A polymer-mediated polyol method was utilized to synthesize the platinum catalysts [12]. Poly(vinylpyrrolidone), PVP, (Aldrich) was employed to prevent particle agglomeration and achieve small and uniform Pt nanoparticles. Briefly, PVP mixed with water was added to a dispersion of the carbon support in ethylene glycol (ethylene glycol/water solution: 3/1 (v/v); PVP:Pt = 0.15 (w/w)). Then, a predetermined amount of the Pt precursor $H_2PtCl_6.6H_2O$ (ca. 40% Pt, Aldrich) was mixed with the dispersion and ultrasonicated. The amount of Pt precursor was adjusted to ensure the desired Pt mass was loaded into the catalyst (v.g. 20 %). The Pt precursor concentration in the solution was kept constant at 0.002 M. The platinum ions were reduced by refluxing the polyol solution (at ~140ºC) for 1 h under continuous magnetic stirring. The prepared catalyst was labeled by adding Pt/ to the nomenclature used for the carbon samples. Carbon black powder (Vulcan XC-72R, Cabot International) with a BET surface area of 270 $m^2 \cdot g^{-1}$ was used as a reference material so that the performance of the catalysts could be compared.

ACCEPTED MANUSCRIPT

The electroactive Pt surface area (ESA), was measured by cyclic voltammetry (CV) using an EG&G Parc Mod. 175 Universal Programmer and a Potentiostat Mod. 101 HQ Instruments. A common three-electrode electrochemical cell was employed in these experiments. The electrolyte was a 0.5 M H_2SO_4 solution. A 0.3 cm diameter glassy carbon stick from Carbone Lorraine was used as working electrode and a platinum wire served as the counter electrode. All the potentials were quoted against the reversible hydrogen electrode (RHE) immersed in the same solution as that used as the electrolyte. The working electrode was polished and washed ultrasonically with ultra-pure water. The catalyst ink, consisting of the catalyst and a Nafion solution (5% w/w, Aldrich) in acetone (10 mg catalyst/L and 33% Nafion), was dropped onto the working electrode and left to dry. During the experiments, nitrogen was bubbled through the solution for the purpose of deaeration for 20 minutes prior to the measurements and this atmosphere was maintained during the experiments. The CVs were recorded at a scan rate of 50 $mV \cdot s^{-1}$ at room temperature. Previously, scans at 200 $mV \cdot s^{-1}$ up to 1.2V has been performed in order to clean the Pt of the catalyst layer.

To estimate the ESA parameter from the CV plots, the following equation was employed: ESA $[cm^2 \cdot g^{-1}$ Pt] = $Q/(m_{Pt} \cdot q_H^0)$, where Q is the electrical charge (mC) measured by integrating the voltammetric curve between 0.05V and 0.45V after correction of the double layer charge, m_{Pt} [g Pt] is the actual loading of Pt into the catalyst, and q_H^0 is the charge for a monolayer of one electron adsorption-desorption process on Pt equal to 0.210 $mC \cdot cm^{-2}$ [12].

To evaluate the activity of the supported catalysts in relation to the methanol electrooxidation, CV experiments at 50 $mV \cdot s^{-1}$ were performed using a EG&G Potentiostat Galvanostat Mod. 263A and a solution of 0.1 M CH_3OH (99.8%, Merck) in 0.5 M H_2SO_4.

ACCEPTED MANUSCRIPT

2.3. Characterization

X-ray diffraction (XRD) patterns of the GCNs were obtained on a Siemens D5000 instrument operating at 40 kV and 20 mA, using CuKα radiation (λ=0.15406 nm). X-ray diffraction (XRD) patterns of the Pt catalysts were obtained on a Seifert JSO-DEBYEFLEX 2002 instrument, using CuKα radiation. Transmission electron micrographs (TEM) and selected area electron diffraction (SAED) patterns of the GCNs were taken on a JEOL (JEM-2000 FX) microscope operating at 200 kV. The dispersion and size of the Pt particles were evaluated by the TEM images (JEOL (JEM-2010) microscope operating at 200 kV). Two to five hundred particles were measured for each sample to obtain statistically significant results. High-resolution transmission electron micrographs (HRTEM) were taken on a JEOL (JEM-3000 F) microscope operating at 300 kV. The Raman spectra were recorded on a Horiva (LabRam HR-800) spectrometer. The source of radiation was a laser operating at a wavelength of 514 nm and a power of 25 mW. The loadings of Pt into the catalysts were determined by thermogravimetric analysis (TGA), which was performed in a Setaram 92-16.18 under air (Heating rate: 10 ºC/min). X-ray photoelectron spectroscopy (XPS) of the catalysts was carried out by means of a VG-Microtech Multilab spectrometer, using MgKα (1253.6 eV) radiation from a double anode with an energy flow of 50 eV. Adsorption measurements of the graphitized carbons were performed using a Micromeritics ASAP 2010 volumetric adsorption system. The external surface area (S_{ext}) was estimated by means of the α_s-plot method employing a nongraphitised carbon black as reference [13].

3. Results and discussion

3.1. Structural properties of graphitic carbon nanostructures (GCNs)

The overall synthesis methodology employed to prepare GCNs using saccharides as precursors is schematically illustrated in Figure 1. During the thermal treatment of the

ACCEPTED MANUSCRIPT

samples impregnated with metallic nitrates the following processes take place: a) decomposition of metallic nitrates to metal oxides (T<240ºC), b) pyrolysis of the saccharides and their transformation into amorphous carbon (T~300-600ºC), c) formation of metallic nanoparticles through the reduction of metal oxides (T~600ºC) and d) transformation of a fraction of amorphous carbon into more ordered graphitic structures (T>700ºC). The graphitic carbon present in these samples is produced from the amorphous carbon that is in contact with the metallic nanoparticles. These nanoparticles act as graphitization catalysts according to a dissolution-precipitation mechanism [5, 14, 15]. Conversely, the carbon matter far away from the metal nanoparticles retains its amorphous structure. In consequence, the material obtained after the heat treatment is made up of metal nanoparticles dispersed throughout the carbonaceous matrix, which consists of a mixture of graphitic and amorphous carbon. The treatment of this material with $KMnO_4$ (dissolved in an acid medium) allows the metallic species and the amorphous carbon to be converted into soluble products. Then, graphitic carbon nanostructures are extracted as a solid residue. We found that the carbonized samples contain a weight ratio of (Amorphous carbon)/(Graphitic carbon)~1-2 and that the yield of GCNs obtained in this way is ~ 7.5 - 11 wt % based on the weight of the saccharide.

The SEM and TEM images obtained for the solid samples extracted after $KMnO_4$ oxidation reveal that they are made up of nanoparticles with a variety of morphologies depending on the precursor and the graphitization catalyst. By means of TEM inspection, we observed that GCNs exhibit similar particle sizes and a very uniform morphology (as an example see Figure 2a). This result contrasts with the high degree of heterogeneity (size and shape) observed for the sawdust-based GCNs and we assume that it is a consequence of that the carbon precursors employed here have a well-defined

ACCEPTED MANUSCRIPT

chemical structure. We also observed that the type of nanostructure originated depends on the metal used as catalyst. In this sense, it is especially remarkable the formation of bamboo-like carbon nanopipes, which were exclusively formed in presence of iron. The SEM microphotograph displayed in Figure 2a clearly shows that they have a filamentous morphology with lengths up to ~1 μm. TEM inspection of these samples reveals their internal structure and show that they consists of bamboo-like nanopipes (see Figures 2b and S2d) with a diameter of ~ 40 nm and well-graphitized walls (see Figure 2c). It is worth mentioning that similar bamboo-like carbon nanopipes have been previously reported [16], but the synthesis methods employed result more complex than that presented here. In contrast to bamboo-like nanopipes obtained from iron, the employ of nickel as catalyst leads to carbon nanostructures with morphologies consisting of nanocoils and nanocapsules. This is illustrated from the images shown in Figure S1 and Figures S2a/b/c (Supporting Information). The carbon nanostructures have a high crystallinity as demonstrated by the high-resolution transmission electronic microscopy images (Figures 2c, S1c and S2e), which display very well defined (002) lattice fringes, and also by the selected area electron diffraction patterns shown in Figure 2d, Figure S1d and Figure S2f.

The X-ray diffraction patterns of the GCNs confirm the high structural order of these materials (Figure 3). Indeed, they exhibit well-resolved XRD peaks at $2\theta \sim 26^{\circ}$, 43º, 54º and 78º, which are assigned to the (002), (10), (004) and (110) diffractions of the graphitic framework, respectively. The structural parameters of these GCNs (i. e. *d*-spacing (002) and the crystallite sizes along the *c*-axis, L_c, and *a*-axis, L_a) are listed in Table 1. The values obtained for the *d*-spacing of ~ 0.339-0.342 nm are larger than the graphite one (0.3354 nm) suggesting distortion occurred in the stacking of the graphene layers (turbostratic structure) [17]. The sizes of the graphitic crystallites L_c and L_a are

ACCEPTED MANUSCRIPT

around 6-10 nm and 10-30 nm respectively. The structural data shown in Table 1 clearly suggest that nickel is a better graphitization catalyst than iron. Variation in the temperature of treatment from 900ºC to 1000ºC does not induce any increase in the structural order. The analysis of the Raman spectra obtained for the GCNs corroborates their high crystallinity and also the superiority of nickel as a graphitization catalyst in relation to iron (see Figure S3 and Table S1 in Supporting Information).

The N_2 sorption isotherms for the GCN samples exhibit large nitrogen adsorption uptakes for relative pressures > 0.9, which is typical of nanosized materials that do not contain framework-confined pores (see Figure S4 in Supporting Information). This result is coherent with the morphology of the GCNs as observed by means of TEM inspection (Figure 2b, Figure S1b and Figures S2b/c/d). For these samples, adsorption only occurs at the outer surface of the nanoparticles and then the specific surface areas match the external surface area. Table 1 contains the values of the external surface area, which are in the 130-180 $m^2 \cdot g^{-1}$ range as deduced by means of the α_s-plot analysis of the N_2 adsorption branch. The application of the α_s-plot to estimate the external surface area is illustrated in Figure S5 (Supporting Information). In general, the values deduced for the external surface area are in agreement with those obtained for the BET surface area (see Table 1). Taking into account that these materials do not contain framework-confined pores, it can be inferred that their external surface area will be easily accessible to reactants, a characteristic that favours their application as electrocatalyst supports.

3.2. Characterization of the Pt/GCN electrocatalysts

TEM microphotographs of the Pt/GCN catalysts show well dispersed Pt nanoparticles over the GNCs (Figure 4). The size of these Pt nanoparticles ranges from ~1 nm to ~5 nm, the mean particle size being in the 2.5-3.0 nm range (Table 2).

ACCEPTED MANUSCRIPT

Moreover, a relatively narrow size distribution of Pt nanoparticles on the GCNs has been achieved, as can be deduced from the size histograms (Figure 4, insets) and from the values obtained for the standard deviations (Table 2).

Figure 5a shows the X-ray diffraction pattern for three representative examples of Pt/GCN samples. All the catalysts exhibit the characteristic diffraction peaks of the fcc structure of platinum [18]. The average particle sizes of Pt/GCNs, determined by applying Scherrer's formula to the (111) diffraction peak, are in the 2.4-3.0 nm range (see Table 2). The average sizes of the particles of all catalysts calculated from the XRD data are consistent with the results obtained by analysis of the TEM micrographs (see Figure 4/insets and Table 2).

The percentage of platinum in the Pt/GCN catalysts was deduced by means of thermogravimetric analysis (see Figure S6 in Supporting Information). They are in the 20.1-21.1 wt % range (see Table 2), which is close to the predicted theoretical amount (20 wt%). The weight loss curves obtained for the oxidation of Pt/Vulcan and several Pt/GCN samples are compared in Figure S6 (Supporting Information). These weight loss profiles clearly show that the carbon supports in the Pt/GCN catalysts have a better stability against oxidation than the Pt/Vulcan sample. This is an important property because it suggests that the Pt/GCN catalytic system will have greater durability [19, 20].

Since metallic platinum is the catalytically active species for hydrogen or methanol electrooxidation [21], it is important to determine the state of oxidation of the platinum nanoparticles deposited on the GCNs. With this purpose, Pt/GCNs were analyzed by X-ray photoelectron spectroscopy (XPS). As an example, in Figure 5b the Pt 4f core level spectra of two representative Pt/GCN samples are shown. In the case of the Pt/CA-2Fe-1000 sample, the Pt 4f line shows a doublet from the spin-orbit splitting of the $4f_{7/2}$

ACCEPTED MANUSCRIPT

(71.2 eV) and $4f_{5/2}$ (74.4 eV) states of metallic Pt (Pt(0)). In contrast, for the Pt/CG-1Fe-900 catalyst, the Pt 4f line consists of two doublets. The most intense doublet observed at 71.1 and 74.4 eV is attributed to the zero valent Pt, while the second doublet at 72.5 and 75.8 eV can be ascribed to the Pt (II) chemical state. The binding energies of the Pt(0) and Pt(II) along with the estimated percentages of both species are presented in Table S2 (Supporting Information) for all catalysts. The high percentages of Pt(0) show that metallic Pt is the predominant species in all the catalysts .

3.3. Electrocatalytic activity of the Pt/GCNs

The electroactive surface area (ESA) of the Pt/GCN catalysts was determined by means of cyclic voltammetry as described in the experimental section. Figure 6a shows some representative examples of the stabilized cyclic voltammograms (CV) measured in a 0.5 M H_2SO_4 solution (scan rate: 50 $mV \cdot s^{-1}$, potential range: 0-1.2 V). The ESA values deduced from the CV plots are summarized in Table 2. All the Pt/GCN catalysts, except Pt/CA-1Ni-900, possess a higher ESA than that measured for the sample used as reference (Pt/Vulcan). The high ESA values of the Pt/GCN catalysts reflect the high degree of dispersion and utilization of Pt nanoparticles, although these supports have a lower BET surface area than Pt/Vulcan. This implies that the surface area of the GCNs is easily accessible, confirming the results obtained by N_2 physisorption. It should also be pointed out that the ESA values measured for the Pt/GCN samples are higher than those reported for electrocatalysts supported on other forms of graphitic carbon, such as mesocarbon microbeads [22], onion-like fullerenes [23], single-wall carbon nanotubes [24] or multiwalled carbon nanotubes [25]. We recently achieved similar ESA values for catalysts made up of Pt nanoparticles deposited on GCNs obtained from pine sawdust [10] and Fe(II) and Co(II) gluconates [11].

ACCEPTED MANUSCRIPT

ACCEPTED MANUSCRIPT

The electrocatalytic activity of the Pt/GCNs towards methanol oxidation was investigated by cyclic voltammetry in a 0.1 M CH_3OH + 0.5 M H_2SO_4 solution. The anodic part of the voltammograms obtained during the 14th cycle (once the double layer contribution has been subtracted) for three representative samples (Pt/CG-1Fe-900, Pt/CA-2Fe-1000 and Pt/CS-1Ni-900) is represented in Figure 6b. The anodic peak obtained in the forward scan at a potential of around 0.79-0.85 V for Pt/GCNs and 0.77 V for Pt/Vulcan is attributed to methanol electrooxidation. Indeed, it is composed of two overlapping oxidation peaks. As shown in Figure 6b (Inset), in the backward scan, the re-oxidation of methanol gives rise to an anodic peak at around 0.69 V. An estimation of the catalytic activity was obtained from the $\mathbf{I_f}$ parameter, which is defined as the current registered at the anodic peak after subtracting the double layer contribution (see Figure 6b). The $\mathbf{I_f}$ data are summarized in Table 2. Interestingly, although Pt/GCNs have a higher proportion of Pt (0) and higher ESA values than Pt/Vulcan, they posses a catalytic activity similar to that of Pt/Vulcan. Normally, a higher ESA value leads to a higher electrocatalytic activity towards methanol oxidation since there is more available Pt area to catalyze the reaction. However, other factors such as the crystallographic surface structure of Pt, have to be considered. It is well-known that the crystallographic orientation of the electrode surface influences the hydrogen and methanol adsorption and electrocatalytic activity of Pt electrodes [26-30]. Depending on the proportion of the different facets in the Pt microcrystallites deposited over the supports, the electrocatalytic activity, as well as the poisoning of the Pt surface, will be different. In this sense, further research would be necessary to explain this behaviour. However, it should be pointed out that the catalytic activities achieved with the Pt/GCNs are higher than the values reported in the literature for electrocatalysts made up of Pt supported on other forms of graphitic carbon, such as multiwalled carbon

ACCEPTED MANUSCRIPT

nanotubes [31, 32]. On the other hand, no functionalization of the supports (contrary to what normally happens with carbon nanotubes [32-36]) has been necessary to achieved good dispersions of Pt nanoparticles.

4. Conclusions

In conclusion, a variety of graphitic carbon nanostructures (nanopipes, nanocoils and nanocapsules) have been prepared by using different saccharides (glucose, sucrose and starch) impregnated with iron or nickel nitrates as precursors. The synthesis method involves two simple steps: a) pyrolysis of the impregnated samples at a moderate temperature (≤1000ºC) and b) oxidation in liquid phase to remove the metallic particles and the amorphous carbon. The solid carbon obtained after oxidation consists of graphitic nanostructures that exhibit a high crystallinity as shown by TEM/SAED, HRTEM, XRD and Raman spectra. Depending on the type of catalyst used, the GCNs formed exhibit a certain morphology, but in all the cases the particle size and the morphology are uniform. It is especially noteworthy the formation of bamboo-like nanopipes, which takes place when the selected catalyst is iron. The use of these nanostructures as electrocatalyst supports provides high dispersions of Pt nanoparticles, which are less than 3.0 nm in size. These electrocatalysts have high electroactive surface areas, in the 70-95 $m^2 \cdot g^{-1}$ Pt range. The measured electrocatalytic activity of the Pt/GCN samples towards methanol electro-oxidation shows that these materials exhibit high activities, which are comparable to that of the Pt/Vulcan system and superior to those measured for other Pt nanoparticles deposited on new carbon forms such as carbon nanotubes (e.g. MWCT).

Acknowledgments. The financial support for this research work provided by the Spanish MCyT (MAT2005-00262, MAT2004-01479 and FEDER) is gratefully acknowledged.

ACCEPTED MANUSCRIPT

M.S. acknowledges the assistance of the Spanish MCyT for the award of a FPU grant. The authors acknowledge J.L. Baldonedo (UCM) for the TEM images of GCNs. C.S. thanks the MEC for a FPU grant.

References

[1] Shenderova OA, Zhirnov VV, Brenner DW. Carbon nanostructures. Crit Rev Sol Stat Mater Sci 2002; 27 (3-4): 227-356.

[2] Bethune DS, Kiang CH, DeVries M, Gorman G, Savoy R, Vazquez J et al. Cobalt-catalysed growth of carbon nanotubes with single-atomic-layer walls. Nature 1993; 363 (6430): 605-7.

[3] Ma Y, Hue Z, Huo K, Lu Y, Hu Y, Liu Y et al. A practical route to the production of carbon nanocages. Carbon 2005; 43 (8): 1667-72.

[4] Cassell AM, Raymakers JA, Kong J, Dai H. Large Scale CVD Synthesis of Single-Walled Carbon Nanotubes. J Phys Chem B 1999; 103 (31): 6484-92.

[5] Oya A, Marsh H. Phenomena of catalytic graphitization. J Mater Sci 1982; 17 (2): 309-22.

[6] Marsh H, Crawford D, Taylor DW. Catalytic graphitization by iron of isotropic carbon from polyfurfuryl alcohol, 725–1090 K. A high resolution electron microscope study. Carbon 1983; 21 (1): 81-7.

[7] Maldonado-Hodar FJ, Moreno-Castilla C, Rivera-Utrilla J, Hanzawa Y, Yamada Y. Catalytic Graphitization of Carbon Aerogels by Transition Metals**.** Langmuir 2000; 16 (9): 4367-73.

[8] Han S, Yun Y, Park KW, Sung YE, Hyeon T. Simple Solid-Phase Synthesis of Hollow Graphitic Nanoparticles and their Application to Direct Methanol Fuel Cell Electrodes. Adv Mater 2003; 15 (22): 1922-5.

ACCEPTED MANUSCRIPT

[9] Sevilla M, Fuertes AB. Catalytic graphitization of templated mesoporous carbons. Carbon 2006; 44 (3): 468-74.

[10] Sevilla M, Sanchís C, Valdés-Solís T, Morallón E, Fuertes AB. Synthesis of Graphitic Carbon Nanostructures from Sawdust and Their Application as Electrocatalyst Supports. J Phys Chem C 2007; 111 (27): 9749-56.

[11] Sevilla M, Salinas Martínez-de Lecea C, Valdes-Solís T, Morallón E, Fuertes AB. Solid-phase synthesis of graphitic carbon nanostructures from iron and cobalt gluconates and their utilization as electrocatalyst supports. Phys Chem Chem Phys, In press, 2007.

[12] Chen M, Xing Y. Polymer-Mediated Synthesis of Highly Dispersed Pt Nanoparticles on Carbon Black. Langmuir 2005; 21 (20): 9334-8.

[13] Kruk M, Jaroniec M, Gadkaree KP. Nitrogen Adsorption Studies of Novel Sy.nthetic Active Carbons. J Colloid Interface Sci 1997; 192 (1): 250-6.

[14] Derbyshire FJ, Presland, AEB, Trimm DL. Graphite formation by the dissolution-precipitation of carbon in cobalt, nickel and iron. Carbon 1975; 13 (2): 111-3.

[15] Krivoruchko OP, Zaikovskii VI. Formation of liquid phase in the carbon–metal system at unusually low temperature. Kinet Catal 1998; 39 (4): 561-70.

[16] Lin M, Tan JPY, Boothroyd C, Loh KP, Tok ES, Foo YL. Dynamical observation of bamboo-like carbon nanotube growth. NanoLett 2007; 7 (8): 2234-2238.

[17] Inagaki, M. New carbons. Control of structure and functions. Elsevier: Amsterdam, 2000.

[18] Fujiwara N, Yasuda K, Ioroi T, Siroma Z. Preparation of platinum-ruthenium onto solid polymer electrolyte membrane and the application to a DMFC anode. Electrochim Acta 2002; 47 (25): 4079-84.

ACCEPTED MANUSCRIPT

ACCEPTED MANUSCRIPT

[19] Knights SD, Colbow KM, St-Pierre J, Wilkinson DP. Aging mechanisms and lifetime of PEFC and DMFC. J Power Sources 2004; 127 (1-2): 127-34.

[20] Stevens DA, Dahn JR. Thermal degradation of the support in carbon-supported platinum electrocatalysts for PEM fuel cells. Carbon 2005; 43 (1): 179-88.

[21] Li H, Sun G, Gao Y, Jiang Q, Jia Z, Xin Q. Effect of Reaction Atmosphere on the Electrocatalytic Activities of Pt/C and PtRu/C Obtained in a Polyol Process. J Phys Chem C 2007; 111 (42): 15192-15200.

[22] Liu YC, Qiu XP, Huang YQ, Zhu WT. Methanol electro-oxidation on mesocarbon microbead supported Pt catalysts. Carbon 2002; 40 (13): 2375-80.

[23] Xu B, Yang X, Wang X, Guo J, Liu X. A novel catalyst support for DMFC: Onion-like fullerenes. J Power Sources 2006, 162 (1):160-4.

[24] Liu Z, Xing YL, Guo B, Hong L, Lee JY. Pt and PtRu nanoparticles deposited on single-wall carbon nanotubes for methanol electro-oxidation. J Power Sources 2007; 167 (2): 272-80.

[25] Xing Y. Synthesis and Electrochemical Characterization of Uniformly-Dispersed High Loading Pt Nanoparticles on Sonochemically-Treated Carbon Nanotubes. J Phys Chem B. 2004; 108 (50): 19255-9.

[26] Lamy C, Leger JM, Clavilier J, Parsons R. Structural effects in electrocatalysis. A comparative study of the oxidation of CO, HCOOC y CH_3OH on single crystal Pt electrodes. J Electroanal Chem 1983; 150 (1-2): 71-77.

[27] Herrero E, Franaszcuk K, Wieckowski A. Electrochemistry of methanol at low index crystal planes of platinum: An integrated voltammetric and chronoamperometric study. J Phys Chem 1994; 98 (19): 5074-5083.

ACCEPTED MANUSCRIPT

[28] Xia XH, Iwasita T, Ge F, Vielstich W. Structural effects and reactivity in methanol oxidation on polycrystalline and single crystal platinum. Electrochim Acta 1996; 41 (5): 711-718.

[29] Tripković A, Gojković SLJ, Popović KDJ, Lović JD. Methanol oxidation at platinum electrodes in acidic solution: comparison between model and real catalysts. J Serb Chem Soc 2006; 71 (12): 1333-1343.

[30] Housmans THM, Wonders AH, Koper, MTM. Structure sensitivity of methanol electrooxidation pathways on platinum: An on-line electrochemical mass spectrometry study. J Phys Chem B 2006; 110 (20): 10021-10031.

[31] Mu Y, Liang H, Hu J, Jiang L, Wan L. Controllable Pt Nanoparticle Deposition on Carbon Nanotubes as an Anode Catalyst for Direct Methanol Fuel Cells. J Phys Chem B. 2005; 109 (47): 22212-6.

[32] Kim Y-T, Mitani T. Surface thiolation of carbon nanotubes as supports: A promising route for the high dispersion of Pt nanoparticles for electrocatalysts. J Catal 2006; 238 (2): 394-401.

[33] Yu R, Chen L, Liu Q, Lin J, Tan K-L, Ng SC, Chan HSO, Xu G-Q, Andy Hor TS. Platinum Deposition on Carbon Nanotubes via Chemical Modification. Chem Mater 1998; 10 (3):718-722.

[34] Guo DJ, Li HL. High dispersion and electrocatalytic properties of Pt nanoparticles on SWNT bundles. J Electroanal Chem 2004; 573 (1): 197-202.

[35] Rajalakshmi N, Ryu H, Shaijumon MM, Ramaprabhu S. Performance of polymer electrolyte membrane fuel cells with carbon nanotubes as oxygen reduction catalyst support material. J Power Sources 2005; 140 (2): 250-257.

ACCEPTED MANUSCRIPT

[36] Wang JJ, Yin GP, Zhang J, Wang ZB, Gao YZ. High utilization platinum deposition on single-walled carbon nanotubes as catalysts for direct methanol fuel cell. Electrochim Acta 2007; 52 (24): 7042-7050.

ACCEPTED MANUSCRIPT

ACCEPTED MANUSCRIPT

Table 1. Structural and textural properties of the graphitic carbon nanostructures.

Precursor	Sample	d_{002} (nm)	L_c (nm)	L_a (nm)	S_{BET} ($m^2 \cdot g^{-1}$)	S_{ext} ($m^2 \cdot g^{-1}$)
Glucose	CG-1Ni-900	0.341	9.8	28	117	162
	CG-1Fe-900	0.342	6.4	14	176	178
	CG-2Fe-1000	0.339	6.5	16	-	-
Sucrose	CS-1Ni-900	0.341	9.8	26	102	133
Starch	CA-1Ni-900	0.342	9.1	17	118	140
	CA-1Ni-1000	0.341	9.4	18	-	-
	CA-2Ni-1000	0.340	9.3	29	98	134
	CA-1Fe-900	0.342	5.8	9.1	-	-
	CA-2Fe-1000	0.339	7.0	16	152	155

ACCEPTED MANUSCRIPT

ACCEPTED MANUSCRIPT

Table 2. Physical properties and catalytic activities towards methanol oxidation of Pt/GCN electroctalysts.

Presursor	Catalyst	Pt (wt %)	Pt size (nm)		EAS ($m^2 \cdot g^{-1}$ Pt)	I_f ($A \cdot g^{-1}$ Pt)
			TEM [a]	XRD		
Glucose	Pt/CG-1Ni-900	21.1	2.5 (0.5)	2.3	80.0	-
	Pt/CG-1Fe-900	21.1	2.6 (0.6)	3.0	94.8	195
Sucrose	Pt/CS-1Ni-900	21.0	2.8 (0.5)	2.4	82.7	182
Starch	Pt/CA-1Ni-900	21.1	2.8 (0.5)	2.5	69.8	-
	Pt/CA-2Ni-1000	20.1	3.0 (0.6)	2.4	85.7	-
	Pt/CA-2Fe-1000	20.7	2.9 (0.5)	2.9	92.1	186
Carbon Black	Pt/Vulcan	20.9	2.6 (0.5)	2.2	73.6	192

[a] Mean Pt size. The standard deviations are indicated in parenthesis.

ACCEPTED MANUSCRIPT

ACCEPTED MANUSCRIPT

Legends

Figure 1. Illustration of the synthetic scheme used to fabricate GCNs by employing different saccharides as precursors.

Figure 2. Microstructure of GCNs obtained from glucose. (a) SEM image (900ºC, Fe), (b) TEM image (900ºC, Fe), (c) HRTEM microphotograph (900ºC, Fe) and (d) SAED pattern (900ºC, Ni).

Figure 3. XRD patterns of the graphitic carbon nanostructures obtained from different saccharides (Catalyst: nickel; T: 900ºC).

Figure 4. TEM images of Pt/GCNs. (a) Pt/CA-2Fe-1000, (b) Pt/CG-1Ni-900 and (c) Pt/CS-1Ni-900. Insets: size histograms of deposited Pt nanoparticles.

Figure 5. (a) XRD patterns of the Pt/GCNs. (b) Pt 4f photoelectron spectra of the Pt/GCNs.

Figure 6. (a) Cyclic voltammograms for the Pt/CG-1Fe-900, Pt/CA-2Ni-1000 and Pt/CS-1Ni-900 catalysts in a 0.5 M H_2SO_4 solution at 50 $mV \cdot s^{-1}$. Inset: zoom of the hydrogen adsorption potential range for Pt/CG-1Fe-900 (thin line) and Pt/CA-2Ni-1000 (thick line). For the sake of clarity, the curve for Pt/CG-1Fe-900 has been vertically shifted by 0.7 $A \cdot g^{-1}$Pt. (b) Anodic part of the cyclic voltammograms (once the double layer contribution has been subtracted) of room-temperature methanol oxidation on Pt/CG-1Fe-900, Pt/CA-2Fe-1000 and Pt/CS-1Ni-900 catalysts in 0.1 M CH_3OH in 0.5 M H_2SO_4 at 50 $mV \cdot s^{-1}$. Inset: Cyclic voltammogram of Pt/CG-1Fe-900.

ACCEPTED MANUSCRIPT

ACCEPTED MANUSCRIPT

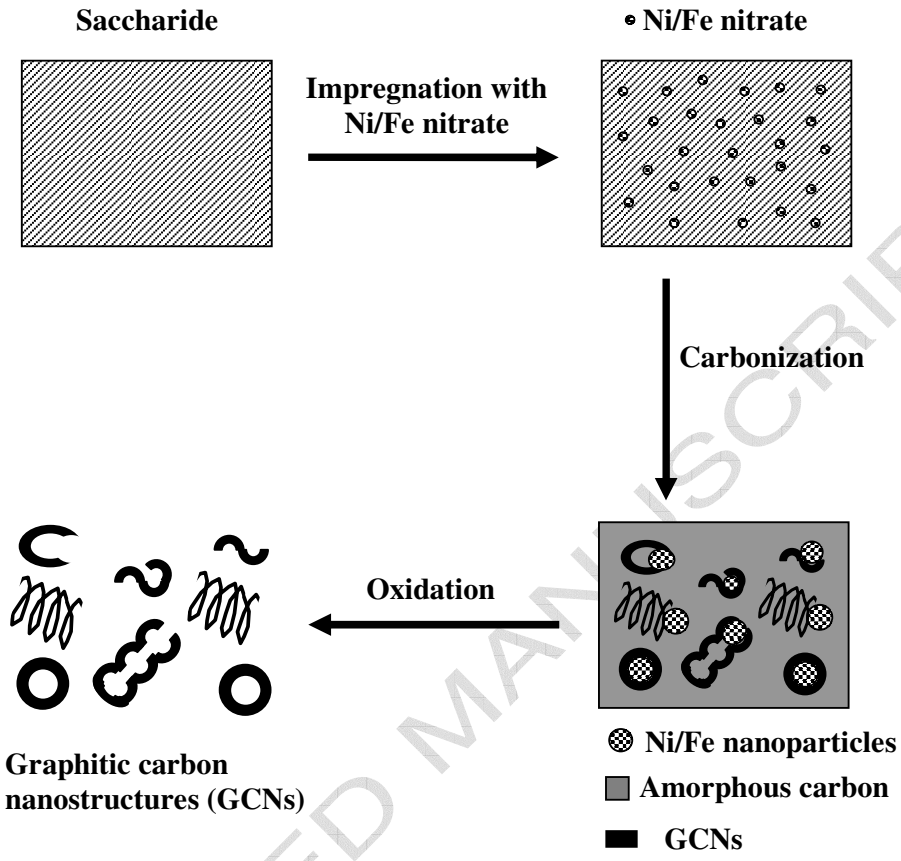

Figure 1

ACCEPTED MANUSCRIPT

ACCEPTED MANUSCRIPT

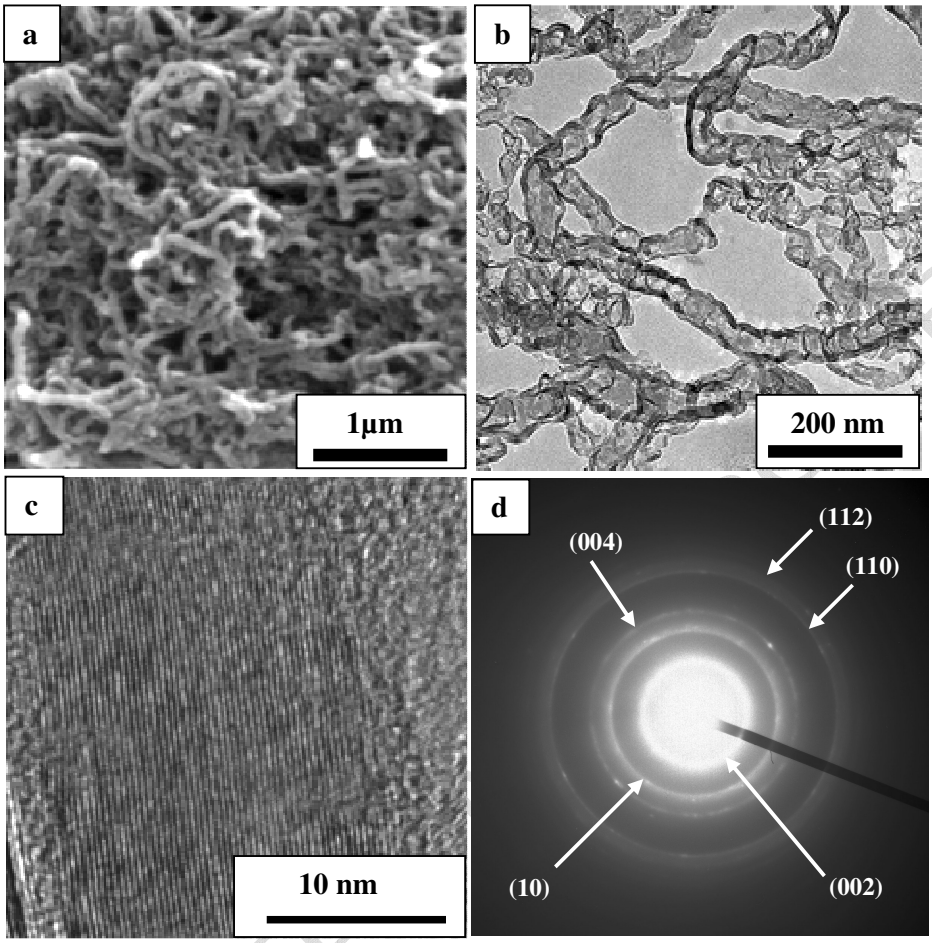

Figure 2

ACCEPTED MANUSCRIPT

ACCEPTED MANUSCRIPT

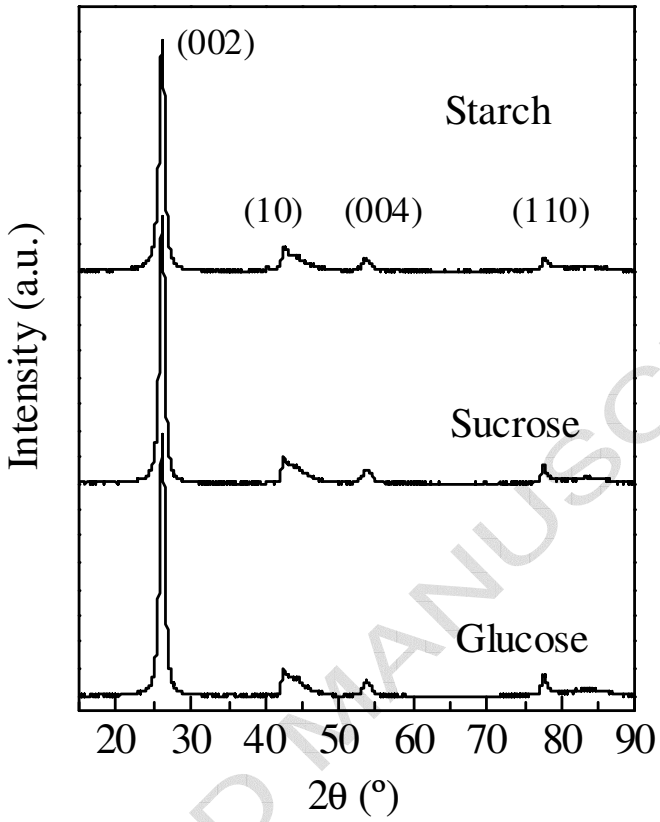

Figure 3

ACCEPTED MANUSCRIPT

ACCEPTED MANUSCRIPT

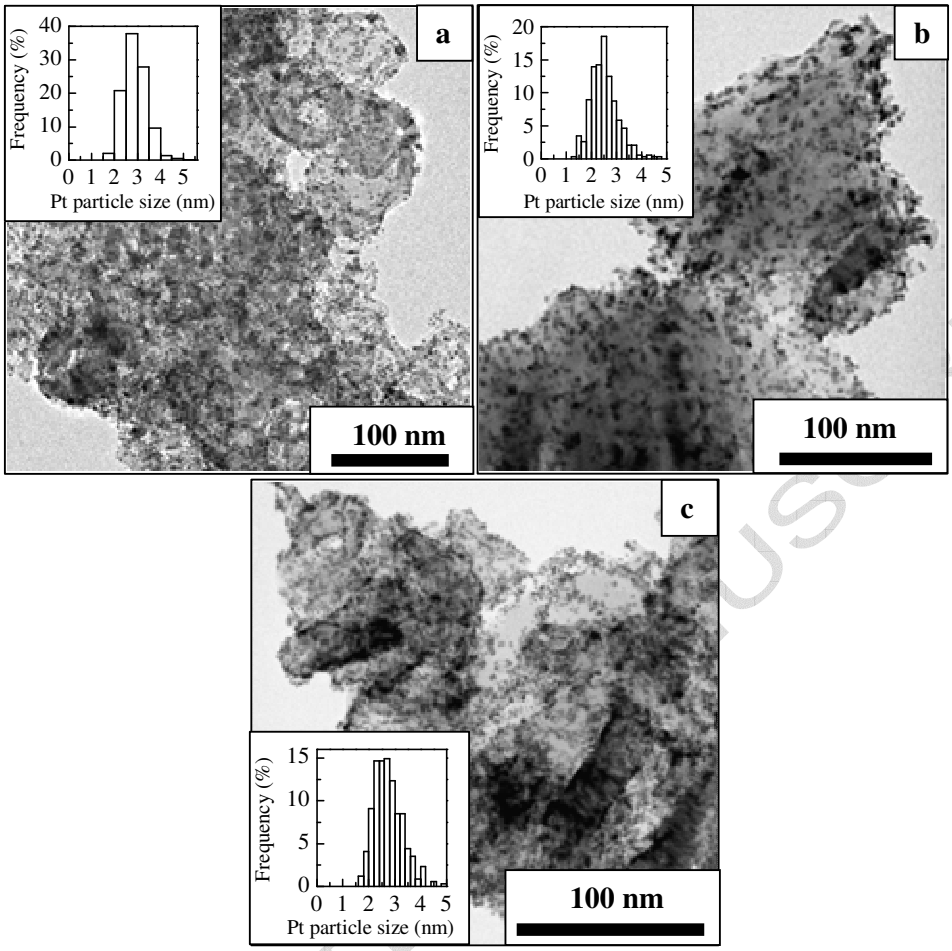

Figure 4

ACCEPTED MANUSCRIPT

ACCEPTED MANUSCRIPT

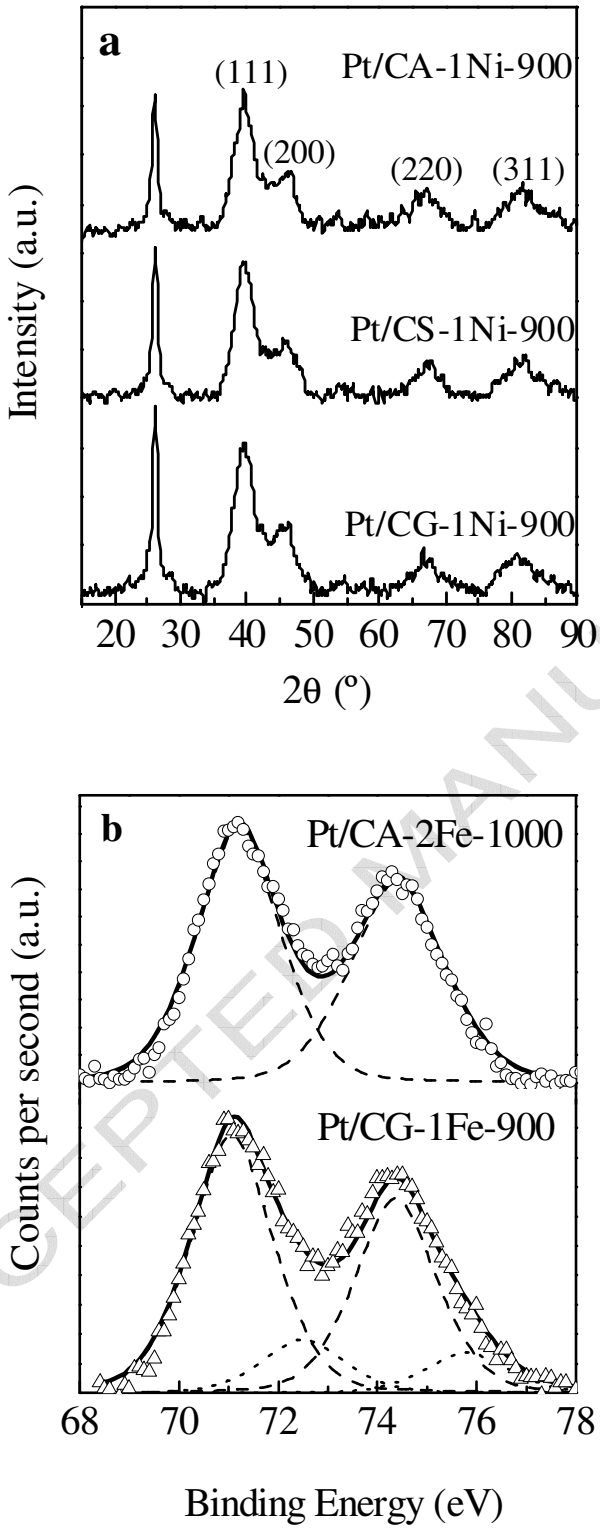

Figure 5

ACCEPTED MANUSCRIPT

ACCEPTED MANUSCRIPT

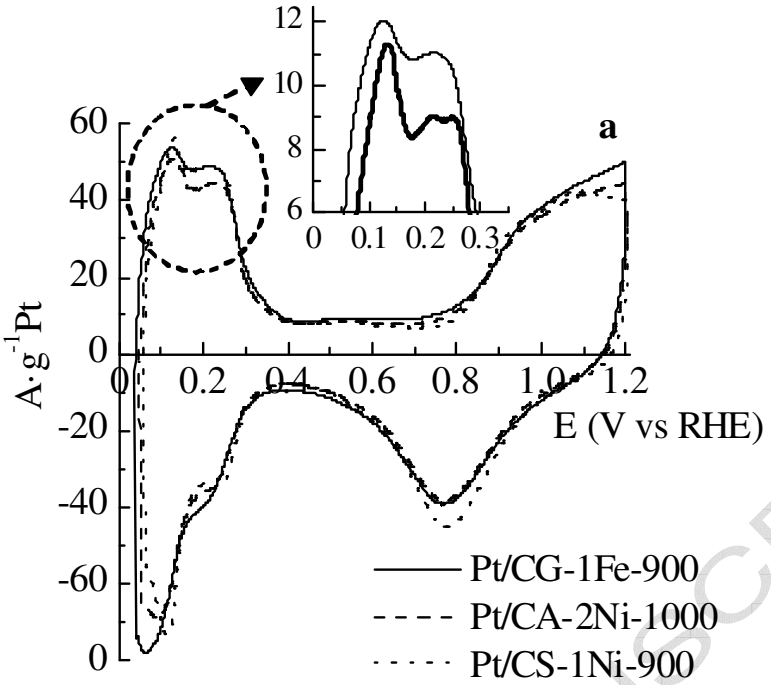

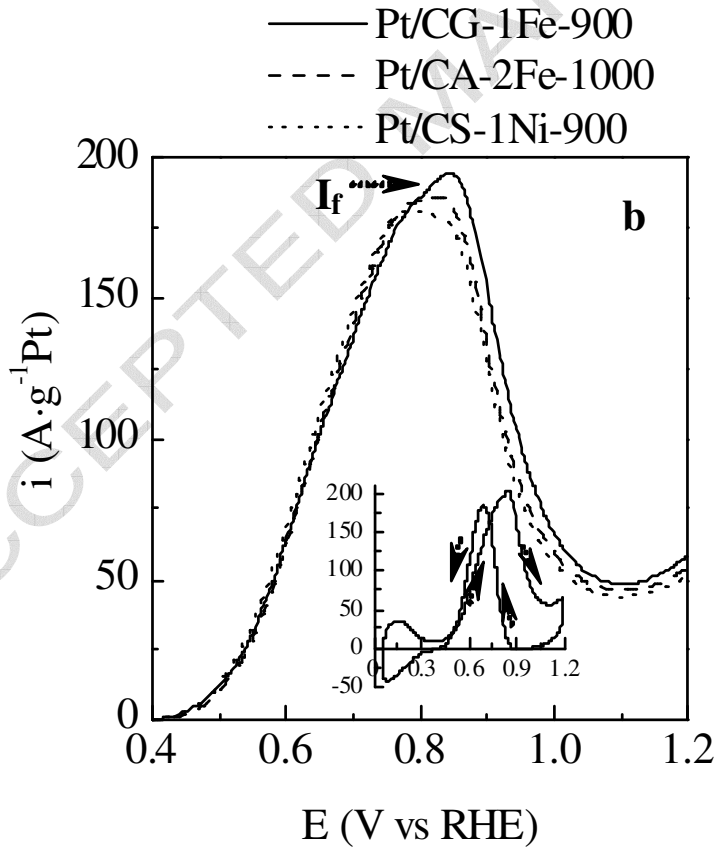

Figure 6

ACCEPTED MANUSCRIPT

ACCEPTED MANUSCRIPT

Supporting Information

Direct synthesis of graphitic carbon nanostructures from saccharides and their use as electrocatalytic supports

M. Sevilla,[a] *C. Sanchís,*[b] *T. Valdés-Solís,*[a] *E. Morallón*[b] *and A. B. Fuertes*[*a]

[a] Instituto Nacional del Carbón (CSIC), P. O. Box 73, 33080-Oviedo, Spain

[b] Departamento de Química Física e Instituto Universitario de Materiales. Universidad de Alicante. Apartado 99. 03080-Alicante. Spain

[*] **Corresponding author.** E-mail**:** abefu@incar.csic.es

ACCEPTED MANUSCRIPT

ACCEPTED MANUSCRIPT

S1. Microscopic analysis of the morphology and structure of the sucrose- and starch-based graphitic carbon nanoparticles

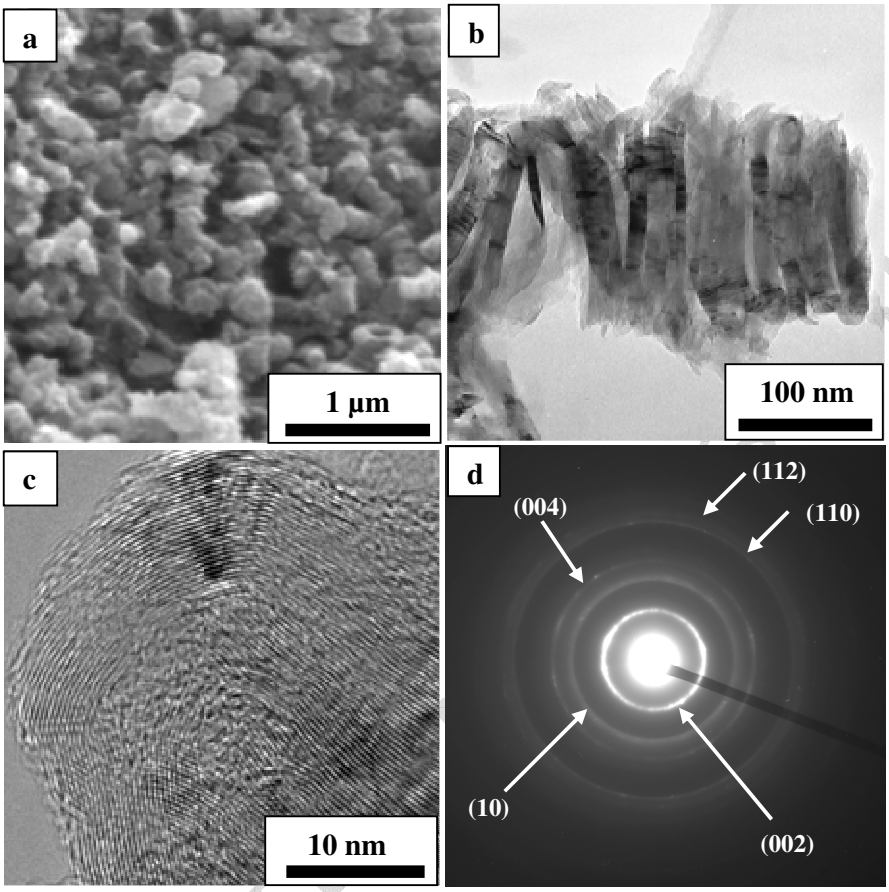

Figure S1. Microstructure of GCNs obtained from sucrose treated at 900ºC in the presence of Ni. (a) SEM image of nanoparticles, (b) TEM image of a nanocoil, (c) HRTEM microphotograph and (d) SAED pattern.

ACCEPTED MANUSCRIPT

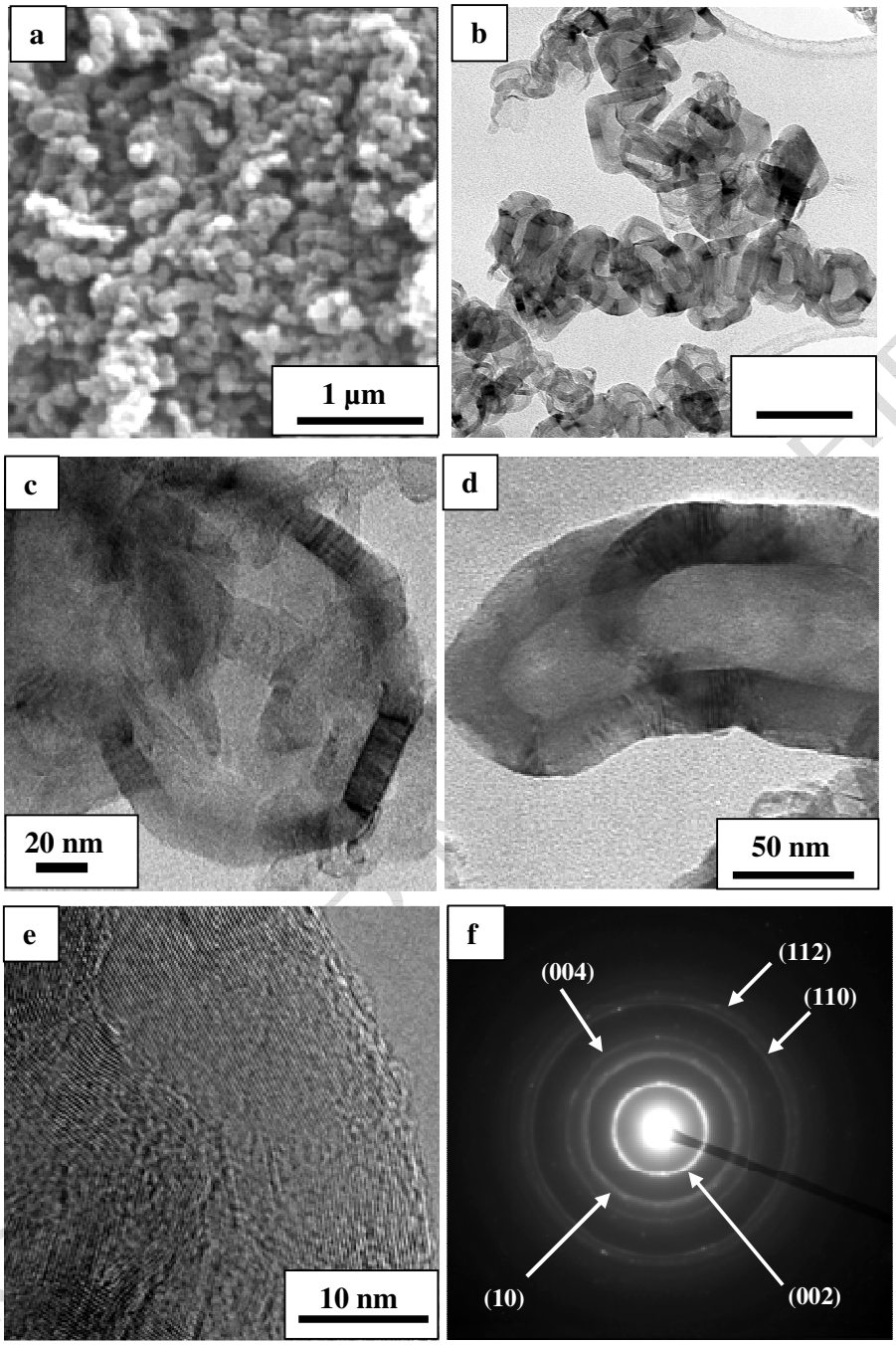

Figure S2. Microstructure of GCNs obtained from starch. (a) SEM image of nanoparticles (900ºC, Ni), (b, c) TEM images of nanocapsules (900ºC, Ni), (d) detail of bamboo-like nanotube (Fe, 1000ºC), (e) HRTEM microphotograph (900ºC, Ni) and (f) SAED pattern (1000ºC, Fe).

ACCEPTED MANUSCRIPT

S2. Raman spectra of the GCNs

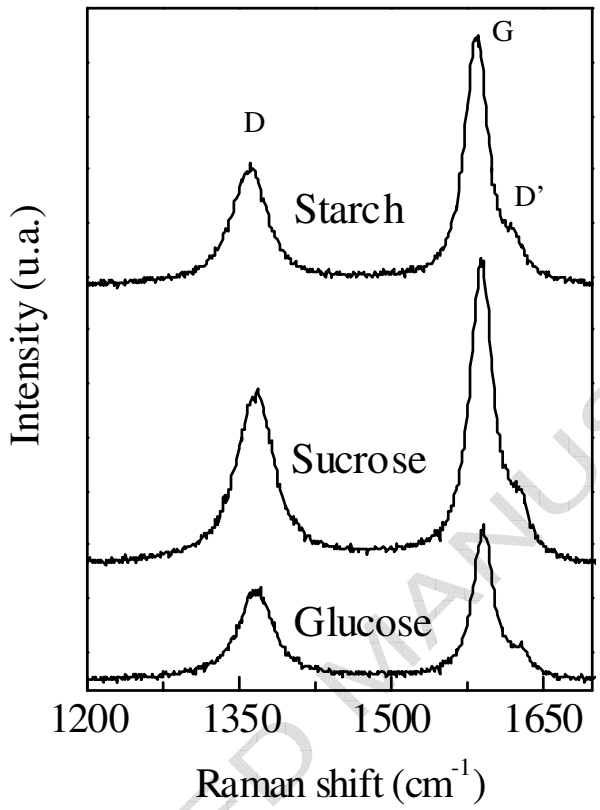

Figure S3. First-order Raman spectra of graphitic carbon nanostructures obtained from different saccharides (Catalyst: Ni; Temperature of pyrolysis: 900ºC).

The first-order Raman spectra obtained for the GCNs corroborate the high crystallinity of these materials (Figure S3). Indeed, they exhibit a high-intensity sharp band at ~1575 cm^{-1} (G band) which is associated to the E_{2g2} vibrational mode of sp^2 bonded carbon atoms (Graphene sheets) and an additional weak band at ~1350 cm^{-1} (D band) which is related to the imperfections in the graphitic sp^2 carbon structures. Another first-order band D' is observed as a shoulder on the G band at ~ 1610 cm^{-1}. Like the G band, the D' band corresponds to a graphitic lattice mode with E_{2g} symmetry [1]. The relative

ACCEPTED MANUSCRIPT

intensity ratio between the D and G bands (I_D/I_G) and the full width at half-maximum of the G band ($\Delta\nu_G$) reflect the degree of graphitization. Low values for the (I_D/I_G) and $\Delta\nu_G$ parameters indicate a high degree of graphitization [2]. The results obtained for the relative intensity of the two peaks (I_D/I_G) and for the $\Delta\nu_G$ parameter clearly point to a high degree of graphitization in the GCNs (see Table S1).

Table S1. Structural parameters of GCNs deduced from an analysis of the Raman spectra.

Precursor	Sample	I_D/I_G	$\Delta\upsilon_G$ (cm^{-1})
Glucose	CG-1Ni-900	0.919	25.7
	CG-1Fe-900	1.21	35.3
	CG-2Fe-1000	1.15	37.2
Sucrose	CS-1Ni-900	0.864	27.1
Starch	CA-1Ni-900	0.755	28.2
	CA-1Ni-1000	0.736	27.4
	CA-2Ni-1000	0.691	26.5
	CA-1Fe-900	1.10	37.4
	CA-2Fe-1000	0.825	31.6

References

[1] Sadezky A, Muckenhuber H, Grothe H, Niessner R, Pöschl U. Raman microspectroscopy of soot and related carbonaceous materials: Spectral analysis and structural information. Carbon 2005; 43 (8): 1731-42.

[2] Lespade P, Marchand A, Couzi M, Cruege F. Caractérisation de matériaux carbonés par microspectrométrie Raman. Carbon 1984; 22 (4-5): 375-85.

ACCEPTED MANUSCRIPT

ACCEPTED MANUSCRIPT

S3. N_2 physisorption analysis of the GCNs

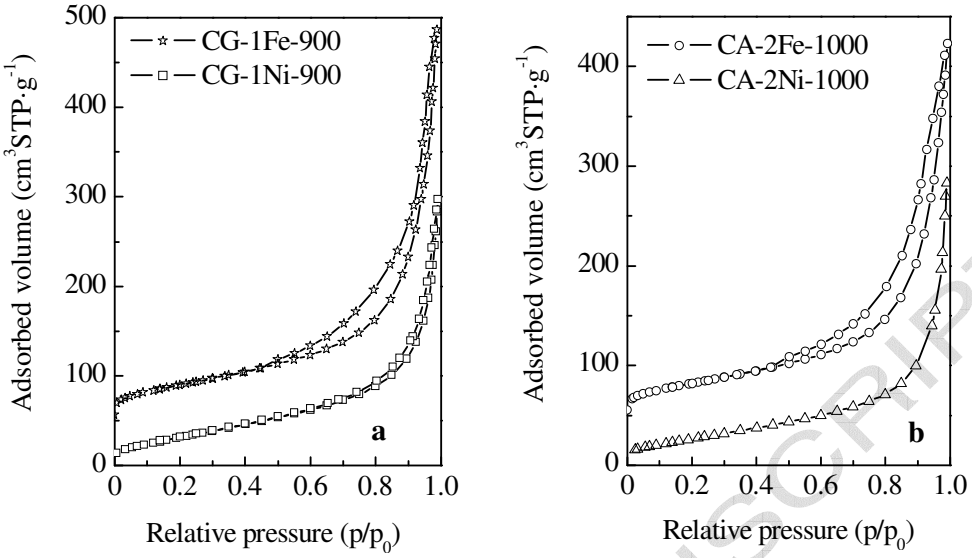

Figure S4. Typical N_2 sorption isotherms for the GCNs obtained from (a) glucose and (b) starch. The graphs of the samples CG-1Fe-900 in a) and CA-2Fe-1000 in b) were vertically shifted 40 $cm^3 \cdot g^{-1}$ for clarity.

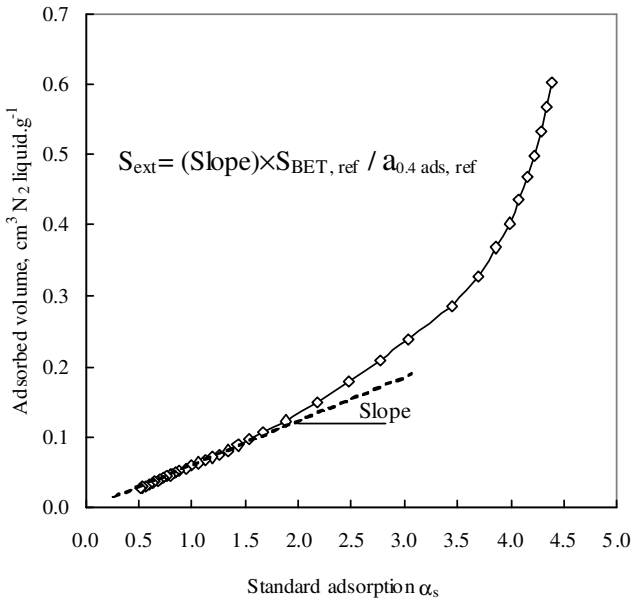

Figure S5. Illustration of the method employed for the calculation of the external surface area. $S_{BET,\ ref}$ is the BET surface area of the material used as reference and $a_{0.4\ ads,\ ref}$ is the amount of nitrogen (cm^3 N_2 liquid.g^{-1}) adsorbed by the reference solid at a relative pressure of 0.4. For details see M. Kruk, M. Jaroniec, K. P. Gadkaree, J. Colloid. Interface Sci. 192 (1997) 250.

ACCEPTED MANUSCRIPT

S4. Thermogravimetric analysis of the Pt/GCN catalysts

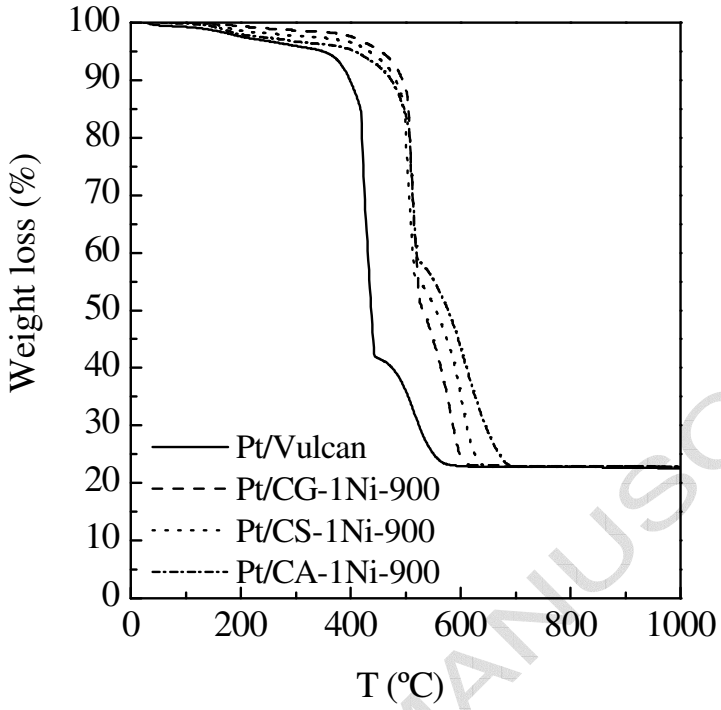

Figure S6. TGA curves of the Pt/GCNs and Pt/Vulcan (Atmosphere: air; heating rate: 5 K/min).

ACCEPTED MANUSCRIPT

ACCEPTED MANUSCRIPT

S5. X-ray photoelectron spectroscopy (XPS)

Table S2. Binding energies (eV) of the Pt (0) and Pt (II) components along with the Pt (0) and Pt (II) contents obtained by XPS characterization.

Sample	Pt_{4f}		Pt (0)/Pt (0+II), %
	Pt(0)	Pt (II)	
Pt/CA-1Ni-900	71.1-74.4	72.5-75.8	71.0
Pt/CA-2Ni-1000	71.2-74.4	-	100
Pt/CA-2Fe-1000	71.2-74.4	-	100
Pt/CG-1Ni-900	71.1-74.4	72.5-75.8	77.2
Pt/CG-1Fe-900	71.1-74.4	72.5-75.8	82.9
Pt/CS-1Ni-900	71.1-74.4	72.5-75.8	78.1
Pt/Vulcan	71.2-74.5	72.5-75.8	70.0

ACCEPTED MANUSCRIPT